THE JOURNAL OF BIOLOGICAL CHEMISTRY VOL. 286, NO. 38, pp. 33358–33368, September 23, 2011

Systematic Identification of Tubulin-interacting Fragments of the Microtubule-associated Protein Tau Leads to a Highly Efficient Promoter of Microtubule Assembly*[S]

Received for publication, January 20, 2011, and in revised form, July 11, 2011 Published, JBC Papers in Press, July 12, 2011, DOI 10.1074/jbc.M111.223545

Caroline Fauquant[‡1], Virginie Redeker[‡], Isabelle Landrieu[§], Jean-Michel Wieruszeski[§], Dries Verdegem[§], Olivier Laprévote[¶], Guy Lippens[§], Benoît Gigant[‡2], and Marcel Knossow[‡3]

From the [‡]Laboratoire d'Enzymologie et Biochimie Structurales, Centre de Recherche de Gif, CNRS, 91198 Gif-sur-Yvette, the [§]Unité de Glycobiologie Structurale et Fonctionnelle, UMR 8576 CNRS, IFR 147, Université des Sciences et Technologies de Lille, 59655 Villeneuve d'Ascq, and the [¶]Laboratoire de Spectrométrie de Masse, Institut de Chimie des Substances Naturelles, Centre de Recherche de Gif, CNRS, 91198 Gif-sur-Yvette, France

Tau is a microtubule-associated protein that stabilizes microtubules and stimulates their assembly. Current descriptions of the tubulin-interacting regions of Tau involve microtubules as the target and result mainly from deletions of Tau domains based on sequence analysis and from NMR spectroscopy experiments. Here, instead of microtubules, we use the complex of two tubulin heterodimers with the stathmin-like domain of the RB3 protein (T_2R) to identify interacting Tau fragments generated by limited proteolysis. We show that fragments in the proline-rich region and in the microtubule-binding repeats domain each interact on their own not only with T_2R but also with microtubules, albeit with moderate affinity. NMR analysis of the interaction with T_2R of constructs in these two regions leads to a fragment, composed of adjacent parts of the microtubule-binding repeat domain and of the proline-rich region, that binds tightly to stabilized microtubules. This demonstrates the synergy of the two Tau regions we identified in the Tau-microtubule interaction. Moreover, we show that this fragment, which binds to two tubulin heterodimers, stimulates efficiently microtubule assembly.

Microtubules (MTs)[4] are cylindrical assemblies of $\alpha\beta$-tubulin heterodimers. They represent, together with actin filaments, the major components of the eukaryotic cytoskeleton. They are involved in important functions such as long range organelle transport or mitotic spindle formation. MTs show an intrinsic dynamic behavior as they constantly undergo phases of assembly and disassembly (1). Their dynamics are regulated by molecules that destabilize them (2) or stabilize them. Tau, an MT-associated protein (MAP) preferentially located in axons (3, 4), belongs to the MAP2/Tau subfamily (5). It stimulates MT assembly, stabilizes them by direct binding, and affects their dynamics. Its functions are mainly regulated by phosphorylation. Tau is also involved in neurodegenerative diseases called tauopathies, of which Alzheimer disease is the best known. In pathological situations, aggregates of hyperphosphorylated Tau assemble into paired helical filament; this hyperphosphorylated state leads to the loss of Tau's biological activity (for details, see Refs. 6–10)).

Tau is a natively unfolded protein (11, 12). It occurs in six isoforms in human brain (ranging from 352 to 441 amino acid residues) resulting from alternative splicing (13–15). It is composed of two main domains (Fig. 1*A*). First, there is a projection domain (Met^1–Tyr^{197}) (residue numbering as in the longest human isoform of Tau) in which an N-terminal extension (with 0, 1, or 2 inserts) and the first part of a proline-rich domain (PR1) are distinguished. Second, the assembly domain (Ser^{198}–Leu^{441}) consists of the second part of the proline-rich domain (PR2), three or four microtubule-binding repeats (MTBR, noted R1 to R4), and a C-terminal extension with an upstream pseudo repeat R′. PR2 and R′ constitute the two flanking regions. MTBR (31 or 32 residues) have similar sequences and consist of an 18-residue imperfect repeat and of a 13- or 14-residue inter-repeat region (ir).

Properties of Tau domains and of their subdomains have been dissected *in vivo* and *in vitro*. Many functions of the projection domain have been described, such as its involvement in Tau's association with the plasma membrane (16) or in Tau enrichment at distal neurites (17). The projection domain also determines the spacing of MTs in Tau-induced MT bundles (18, 19) either through some repulsive force as proposed in the case of class II MAPs (20) or via its antiparallel association with the projection domain of another Tau monomer as proposed by Rosenberg *et al.* (21). In the assembly domain, the properties of repeats and of flanking regions have been most extensively characterized. Repeats are required for MT binding and for MT

* This work was supported by the CNRS, Agence Nationale pour la Recherche Grant ANR-05-Blanc-6320-01, Très Grands Equipments RMN THC Fr3050, and Fondation pour la Recherche Médicale Grant DEQ20081213979.

[S] The on-line version of this article (available at http://www.jbc.org) contains supplemental Tables S1 and S2 and Figs. S1 and S2.

[1] Present address: CNRS UMR 5249 Laboratoire de Chimie et Biologie des Métaux; Commissariat à l'Energie Atomique, Direction des Sciences du Vivant, Institut de Recherches en Technologies et Sciences pour le Vivant; Université Joseph Fourier, 17 Ave. des Martyrs, 38054 Grenoble Cedex 9, France.

[2] To whom correspondence may be addressed: Laboratoire d'Enzymologie et Biochimie Structurales, CNRS, 1 Ave. de la Terrasse, F-91198 Gif-sur-Yvette, France. Fax: 33-1-69-82-31-29; E-mail: gigant@lebs.cnrs-gif.fr.

[3] To whom correspondence may be addressed: Laboratoire d'Enzymologie et Biochimie Structurales, CNRS, 1 Ave. de la Terrasse, F-91198 Gif-sur-Yvette, France. Fax: 33-1-69-82-31-29; E-mail: knossow@lebs.cnrs-gif.fr.

[4] The abbreviations used are: MT, microtubule; Cc, Critical concentration; ir, inter repeat; MAP, microtubule-associated protein; MTBR, microtubule-binding repeat; RB3-SLD, RB3-Stathmin like domain; SEC, size exclusion chromatography; Tricine, *N*-[2-hydroxy-1,1-bis(hydroxymethyl)ethyl]glycine.

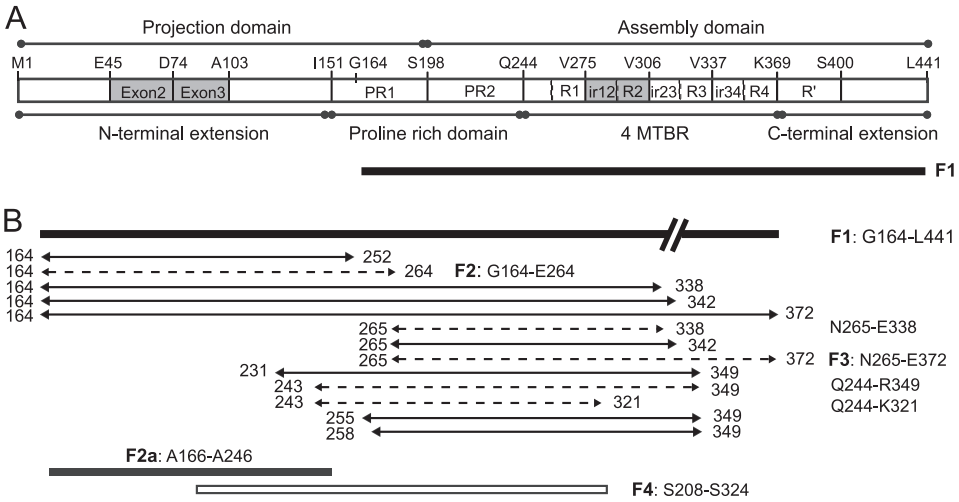

FIGURE 1. **Domain organization of Tau and the fragments of F1 that interact with T_2R.** *A,* domain organization of Tau. *Gray boxes* represent domains that are spliced in some isoforms. Residue numbering is as in the longest human isoform of Tau. In the projection domain, an N-terminal extension and the first part of a proline-rich domain (*PR1*) are distinguished. The assembly domain consists of the second part of the proline-rich domain (*PR2*), three or four MTBRs, and a C-terminal extension with an upstream pseudo repeat R′. The MTBRs are divided in repeats (*R1* to *R4*) and inter-repeats (*ir12*, *ir23*, and *ir34*). The position of F1 (Gly^{164}–Leu^{441}) in Tau sequence is also presented. *B,* F1 fragments that interact with T_2R. These were generated by digestion of F1 either by Glu-C or by Arg-C. The fragments identified in this work are shown as *double arrowed lines*. The affinities for MTs of fragments presented as *double arrowed dashed lines* have been assayed qualitatively, but only named fragments (*F2*, *F3*, *F2a*, and *F4*) have been characterized further. F2a (*black box*) corresponds to the part of F2 that is included in the proline-rich domain. F4 has been produced based on the NMR identification of the residues in the PR2 and MTBR domains that interact with T_2R. It is shown as a *white box*.

assembly. Paradoxically, although MTBR are considered as the MT binding domain, they bind MTs weakly. Binding of PR2 (associated with the projection domain) and of R′, taken individually, was almost beyond detection (22). By contrast, the flanking regions bind strongly to MTs, when combined with the projection domain and the C-terminal extension (22), and influence MT assembly (23, 24).

Two models have been proposed to describe the respective roles of MTBR and flanking regions. In the first one, termed the "jaws" model (22, 25, 26), these last regions allow tight binding of Tau to the MT surface and the presence of repeats is required to favor MT assembly. An NMR study has allowed the determination of the residues in PR2 and in the downstream repeats that constitute the jaws (27). The second model relates to the importance of regions in the assembly domain for the effect of the different Tau isoforms on MT dynamics. It proposes that the initial binding of Tau to MTs is mediated by an MT-binding core within MTBR, whereas the flanking regions exert an isoform-specific regulation (28). The core is composed of the first two repeats and of their inter-repeat (28, 29). Regions in the proline-rich domain (23, 24) modulate MT binding and assembly, but they must be associated with repeats in the same fragment to have an effect. The contribution of basic residues has also been investigated. This identified several of them in the proline-rich domain and in ir12 as important for Tau interaction with MTs (24, 29). Consistent with the basic nature of these residues, cross-linking suggests that the binding targets of repeat 1 and/or ir12 are the C-terminal acid tails of both α- and β-tubulin (30).

Thus, current descriptions of Tau-MT interaction rely on deletions of Tau domains based on sequence analysis, on site-directed mutagenesis of basic residues, and on synthetic peptides. More recently, NMR has been used to define the MT-interacting residues of some Tau fragments (27, 31, 32). In a very different approach, short tubulin-binding peptides have been selected from a phage library and subsequently used to identify tubulin-binding domains in MAPs using sequence comparison (33). Here, we take advantage of the unfolded structure of native Tau so that fragments produced by limited proteolysis should be structurally similar to their counterpart in the whole protein. Similarly to the systematic approach used previously to define the tubulin-binding region of stathmin (34), another natively unfolded protein, we directly identify the Tau proteolysis products that interact with tubulin. The target used here is the complex (T_2R) composed of two tubulin heterodimers with the stathmin-like domain of RB3 (RB3-SLD) (35, 36). The peptides identified, which have a moderate but definite affinity for MTs, define two nonoverlapping domains included in the MTBR and in the proline-rich domains. The tightest binding fragments in each of these regions stimulate assembly. NMR studies of two adjacent fragments, one in the proline-rich domain and one in the MTBR domain, in complex with T_2R identify tubulin-interacting residues within these regions. By combining them in one protein, we produced a 117-amino acid construct (F4, Ser^{208}–Ser^{324}) that binds tightly to MTs and favors their assembly, thus recapitulating two important characteristics of the Tau-tubulin interaction.

EXPERIMENTAL PROCEDURES

Cloning and Site-directed Mutagenesis—The coding region of the full-length 441-residue Tau protein was inserted into a pET15b expression vector (Novagen) as described by Amniai *et al.* (37). The coding region for Tau-(Gly^{164}–Leu^{441}) (F1) described in Sillen *et al.* (32) was subcloned in a pET9aM vector modified in its multiple cloning site, between the restriction sites NdeI and NotI. Two constructions were produced, one with a sequence encoding a His_6 tag at the N-terminal end of F1 (F1-Nt) and the other one with the same motif at the C-terminal

end (F1-Ct). The coding region for Tau-(Ala^{166}–Ala^{246}) (F2a) was inserted in a pET15b vector between the restriction sites NcoI and XhoI. The coding region for Tau-(Asn^{265}–Glu^{372}) (F3) was inserted in the pET9aM vector between the restriction sites NdeI and NotI with primers 5′-CATATGAACCTGAAGCACCAGCCG and 5′-GCGGCCGCTTGTGCTATTCAATC, yielding p*F3*. The coding region for Tau-(Ser^{208}–Ser^{324}) (F4) was inserted in the pET9aM vector between the restriction sites NdeI and NotI with primers 5′-GGGAACATATGCATCACCATCACCATCACAGCCGCTCCCGCACCCCG and 5′-TTTTTGCGGCCGCTTATGAGCCACACTTGGAGG. The coding region for Tau-(Ser^{208}–Ser^{324}) with the residue cysteine 322 mutated in serine (F4 C322S) was inserted in the pET9aM vector between the restriction sites NdeI and NotI with primers 5′-GGGAACATATGCATCACCATCACCATCACAGCCGCTCCCGCACCCCG and 5′-TTTTTGCGGCCGCTTATGAGCCACTCTTGGAGG. A plasmid coding for Tau-(Gln^{244}–Glu^{372}) (K18) was a gift of Kenneth S. Kosik, and the coding region was inserted between NdeI and EcoRI sites in an expression vector with an ampicillin resistance gene. Cloning of additional fragments used in this work is described in the supplemental material. The sequences of all plasmids produced were verified (Eurofin MWG Operon, Germany).

Tubulin Purification—Sheep brain tubulin was purified by two cycles of polymerization/depolymerization in a high molarity buffer (38) and stored in liquid N_2 in 50 mM Mes-K, pH 6.8, 33% glycerol, 0.25 mM $MgCl_2$, 0.5 mM EGTA, 0.1 mM GTP until use. Before use, an additional MT assembly/disassembly cycle was performed to remove any nonfunctional protein. To prepare tubulin for T_2R production, the disassembly step was carried out in 80 mM Pipes-K, pH 6.8, 1 mM $MgCl_2$, 0.5 mM EGTA, 1 mM GDP at 4 °C for 20 min. After ultracentrifugation at 350,000 × *g*, 4 °C for 10 min, the tubulin buffer was exchanged using a PD10 column (GE Healthcare). To prepare tubulin for polymerization and partition assays, the disassembly step was carried out in 15 mM Mes-K, pH 6.8, 0.5 mM $MgCl_2$, 0.5 mM EGTA at 4 °C for 20 min. After ultracentrifugation at 350,000 × *g*, 4 °C for 10 min, 10-μl tubulin fractions were stored in liquid N_2 until use. Tubulin concentrations were deduced from its absorbance (ϵ_{278} = 1.2 liters·cm^{-1}·g^{-1}), assuming the molecular weight of the heterodimer is 100 kDa (39, 40).

Protein Overexpression and Purification—The recombinant RB3-SLD was produced and purified as described previously (41). RB3-SLD concentration was determined by amino acid analysis or by a colorimetric assay with the Thermo Scientific Pierce BCA protein assay Kit, by comparison with an RB3-SLD sample of known concentration used as a standard. F1-Nt or F1-Ct was overexpressed in freshly transformed *Escherichia coli* BL21(DE3) competent cells. Overnight cultures were diluted to A_{600} 0.1 in 3-liter flasks containing 1 liter of 2YT medium supplemented with kanamycin (50 μg·ml^{-1}). Cells growing at 37 °C were induced with 0.5 mM isopropyl β-D-1-thiogalactopyranoside for 3 h when the A_{600} reached 0.6. The cells were harvested by centrifugation at 5000 × *g* for 10 min, resuspended immediately in sonication buffer (50 mM sodium phosphate, pH 7, 1 M NaCl, and 1 tablet of the complete antiprotease mixture (Roche Applied Science)), and lysed by sonication on ice. The lysate was centrifuged at 20,000 × *g* for 20 min at 4 °C. The supernatant was then heated to 75 °C for 10 min before centrifugation at 20,000 × *g* for 20 min at 4 °C. Before loading the protein mixture on a HisTrap column (1 × 5 ml) (GE Healthcare) equilibrated with buffer A (50 mM sodium phosphate, pH 7, 1 M NaCl, 10 mM imidazole), imidazole (10 mM final concentration) was added to the supernatant. The column was washed with 5% buffer B (50 mM sodium phosphate, pH 7, 1 M NaCl, 500 mM imidazole). Protein was eluted with 50% buffer B. After concentration by ultrafiltration (Vivaspin 15 ml, 10-kDa cutoff; Sartorius), F1 was treated with 2 mM DTT, and 5 mM EGTA and then purified on a gel filtration column (Superdex 75 prep grade HR16/60; GE Healthcare) equilibrated with 20 mM sodium phosphate, pH 7, 100 mM NaCl. Tau and Tau fragments with no tag were purified with a cation-exchange column (SP-Sepharose column or Hitrap SP FF columns, GE Healthcare) followed by size exclusion chromatography (SEC) (Superdex 75 preparation grade HR16/60; GE Healthcare). F4 and its single mutant F4 C322S, with a His_6 tag sequence at the N-terminal end, were purified on a HisTrap column (1 × 5 ml) (GE Healthcare) followed by SEC (for details see supplemental material). The purity and identity of Tau fragments were verified by SDS-PAGE and mass spectrometry. The N-terminal methionine was quantitatively removed in F1-Ct, F2, and F2a, partially in F3; it is present in F1-Nt, F4, and K18. Protein concentrations were determined by amino acid content analysis following complete acid hydrolysis.

Limited Proteolysis—Two enzymes, Arg-C and Glu-C (sequencing grade proteases, Roche Applied Science), were selected because of their high number of cleavage sites distributed along the F1 sequence (supplemental Fig. S1*A*). These enzymes were used at a 1:2000 enzyme/F1 ratio (w/w) in the following buffers: 80 mM Pipes-K, pH 6.8, 5 mM $MgCl_2$, 1 mM EGTA, 1 mM DTT, 5 mM $CaCl_2$ (Arg-C) and 25 mM NH_4HCO_3, pH 7.8 (Glu-C). Protein samples were incubated at 37 °C with Arg-C or at room temperature with Glu-C. Incubation times were as follows: 60 min (Arg-C and Glu-C), 90 min (Arg-C), and 180 min (Glu-C). Digestion was stopped by heating at 110 °C for 15 min. F1 proteolysis was monitored by SDS-PAGE (supplemental Fig. S1, *B* and *C*), by SEC, and by mass spectrometry. The F1 cleavage sites were identified after determination of the molecular masses of the fragments, taking into account the F1 amino acid sequence and the cleavage specificities of the endoproteinases.

Mass Spectrometric Identification of F1 Fragments That Interact with T_2R—F1 fragments obtained by proteolysis were incubated with T_2R at a ratio ranging from 0.8:1 to 1:1 for 10 min in ice. The sample (100 or 200 μl) was then loaded on a Superose 12 10/300 column (GE Healthcare) equilibrated with 20 mM Pipes-K, pH 6.8, 1 mM $MgCl_2$, 0.5 mM EGTA and eluted at 0.5 ml/min flow rate. Products eluted from the gel filtration column were collected, analyzed by SDS-PAGE with silver staining, and by matrix-assisted laser desorption/ionization time-of-flight mass spectrometry (MALDI-TOF MS). Digested F1 and (digested F1):T_2R (1-μl samples before SEC) were acidified by dilution in 0.1% trifluoroacetic acid (TFA) before being desalted and eluted in 10 μl of 50% acetonitrile in 0.1% TFA using Zip-Tip® C4 (Millipore). The SEC-eluted fractions following digestion (60 μl acidified with 6 μl 1% TFA) were

desalted and concentrated on a Zip-Tip® C4 or C18 (Millipore) by eluting with 6 μl of 50% acetonitrile in 0.1% TFA. Desalted samples were mixed (1:1) either with a 10 mg/ml solution of sinapinic acid (3,5-dimethoxy-4-hydroxycinnamic acid, Aldrich) in 30% acetonitrile, 0.1% TFA, or with a 10 mg/ml solution of 2,5-dihydroxybenzoic acid (Fluka) in 0.1% TFA. The spectra of positive ions were recorded in linear mode and in reflectron mode using a MALDI-TOF mass spectrometer (Voyager DE-STR, Applied Biosystems). The linear mode was used to measure the average masses of large peptide fragments in the 1000–40,000 mass range, whereas the reflectron mode was used to measure the monoisotopic masses of small peptide fragments in the 500–10,000 mass range. In linear mode, two calibrations were performed: an external calibration with the PepMix 3 kit (Laserbiolabs) mixed with ACTH clip (18–39) (Laserbiolabs) and an internal calibration in the case of samples containing RB3-SLD, using the monoprotonated and biprotonated ions (average *m/z* ratios 16,722.90 and 8361.95, respectively) (42). In reflectron mode, an external calibration was performed with the PepMix 4 kit (Laserbiolabs).

NMR Spectroscopy—^{1}H-^{15}N HSQC spectra were recorded on a Bruker Avance 600-MHz spectrometer equipped with a cryogenic triple resonance probe head or on a Bruker Avance 800-MHz spectrometer with a regular TXI probe head. Samples of the isolated fragments contained 50 μM ^{15}N- and ^{13}C-labeled F1, 52.5 μM ^{15}N-labeled F2a, or 51 μM ^{15}N-labeled K18 in 25 mM Tris-d_{11}, pH 6.7, 25 mM NaCl, 2.5 mM EDTA and 1.5 mM DTT. Assignments were based on the published assignments of K32 (Ser^{198}–Tyr^{394}) (27) for K18 and were verified by the product-plane approach developed in our laboratory (43) on a doubly labeled fragment. The assignment of F2a, presented in the supplemental material, was obtained with the same approach. Some resonances in the extreme C terminus of F1 (Fig. 2) could be assigned in the same manner. For complexes with T_2R, ratios were 30 μM F1, 55 μM T_2R, 53 μM F2a, 73 μM T_2R, and 50 μM K18, 58 μM T_2R. Chemical shift differences between the isolated F2a and F2a in complex with T_2R were calculated as $\Delta\omega = (\Delta\omega_H{}^2 + 0.2\,\Delta\omega_N{}^2)^{1/2}$. For the sample of F1 bound to stabilized MTs, we used 10 μM F1, 40 μM polymerized tubulin but acquired the spectrum with 256 scans instead of 64 for the other spectra. ^{1}H-^{15}N HSQC spectra were acquired with the standard Bruker pulse program, with 2k and 256 complex points in the ^{1}H and ^{15}N directions, respectively. All spectra were recorded at 20 °C.

Binding to Stabilized MTs—Stabilized MTs were produced by incubating tubulin with a concentration of docetaxel equal to twice that of tubulin at 37 °C for 15 min in 50 mM Mes-K, pH 6.8, 6 mM $MgCl_2$, 0.5 mM GTP, 30% glycerol (v/v) (M2G2) or in M2G1 (as M2G2 but with 12.5% glycerol (v/v)), following which Tau fragments at concentrations in the 5–60 μM range were added. Samples were incubated for a further 15 min and then centrifuged (280,000 × *g*, 34 °C, 15 min). The pellets and supernatants were subjected to SDS-PAGE for evaluation of the amounts of MT-bound and free Tau fragments. Gels (Tris/Tricine, 12% acrylamide in the separating gel) were stained with Coomassie Brilliant Blue, scanned, and analyzed using the MultiGauge Version 3.0 software. The measurements were linear up to 2 μg of Tau fragments loaded. In the case of F4, Coomassie Blue staining was not sensitive enough because of the tight binding of this fragment to MTs. Instead, the C322S mutant of F4 labeled with a fluorescent probe was used and quantified with the Las-3000 imager (Fuji Film, filter Y515-Di). Briefly, prior to labeling F4 C322S (150 μM) was reduced by tris(2-carboxyethyl)phosphine (500 μM) in 15 mM Mes-K, pH 6.8, 500 μM EGTA, 500 μM $MgCl_2$ for 30 min at room temperature. A 5-fold excess of Oregon Green 488® maleimide (Invitrogen) was added, and the sample was incubated for 2 h at room temperature in the dark. Finally, the excess dye was removed by buffer exchange using a Micro BioSpin® 6 column (Bio-Rad). Full-length Tau and Tau fragments in the presence of docetaxel but without MTs are exclusively found in the supernatant (data not shown).

Binding parameters of Tau fragments to docetaxel-stabilized MTs were determined by fitting data using the standard binding equation considering two nonequivalent sites (Equation 1),

$$\frac{[\text{Tau}]_{\text{bound}}}{[\text{MTs}]} = \frac{n_1 \cdot K_1 \cdot [\text{Tau}]_{\text{free}} + n_2 \cdot K_2 \cdot [\text{Tau}]_{\text{free}} + (n_1 + n_2) \cdot K_1 \cdot K_2 \cdot [\text{Tau}]_{\text{free}}{}^2}{1 + K_2 \cdot [\text{Tau}]_{\text{free}} + K_1 \cdot [\text{Tau}]_{\text{free}} + K_1 \cdot K_2 \cdot [\text{Tau}]_{\text{free}}{}^2} \quad \text{(Eq. 1)}$$

where [MTs] is the concentration of polymerized tubulin (here it is constant, 25 μM unless otherwise specified) and *n* is the stoichiometry of each site. K_1 and K_2 are the equilibrium constants for association at the two binding sites. Results are the average of triplicate experiments.

To compare binding to MTs and to T_2R, duplicate spin-down assays were run in parallel, in the presence of T_2R or not. Stabilized MTs were produced as described above, in M2G1, from tubulin (25 μM). Stabilized MTs and T_2R were produced together by incubating tubulin (50 μM) with docetaxel (0.55 eq) and RB3-SLD (0.35 eq) at 37 °C for 15 min in M2G1. Samples were incubated for a further 15 min with Tau fragments (10 μM) and centrifuged (280,000 × g, 34 °C, 15 min). Pellets and supernatants were subjected to SDS-PAGE to evaluate the partition of Tau fragments.

Microtubule Assembly—MT assembly was monitored turbidimetrically at 340 nm with a Cary 50 spectrophotometer (Varian) using a 200-μl, 0.7-cm light path cuvette thermostated at 37 °C. Experiments were carried out either in M2G2 or in M2G1 with varying concentrations of reduced Tau fragments. For critical concentration (Cc) determination, tubulin at various concentrations was incubated at 37 °C until the steady state had been reached (as judged by identical samples analyzed in parallel by turbidimetry) and then centrifuged at 250,000 × *g*, 34 °C, for 10 min. Microtubular tubulin is the difference between initial tubulin and the amount in the supernatant. The plot of assembled tubulin as a function of the total tubulin concentration yields a linear curve in the concentration range investigated. The abscissa intercept (Cc) represents the concentration of unassembled tubulin at steady state in the presence of Tau fragments. Cc was 3 μM ± 1 in M2G2 and 14.5 μM ± 4 in M2G1.

Electron Microscopy—MT assembly (tubulin 13 μM) was carried out in M2G1 at 37 °C in the absence or in presence of 5 μM Tau fragments. The sample on a carbon-coated grid was

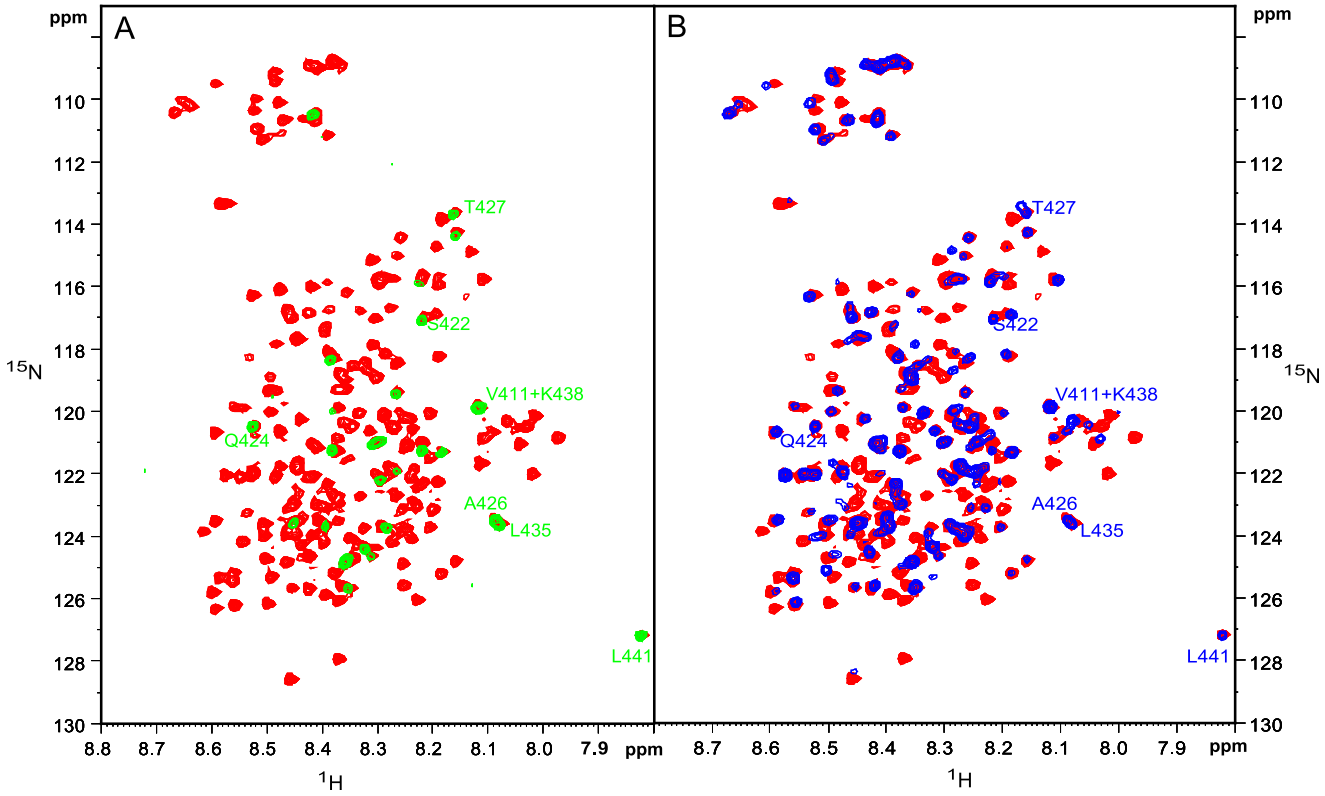

FIGURE 2. **NMR spectra of fragment F1.** ^{1}H,^{15}N HSQC spectrum of F1 when isolated in solution (*red*), in complex with stabilized MTs (*A, green*), or with T_2R (*B, blue*). Peaks visible in the F1/MT sample concern mainly the extreme C terminus of F1 and do not shift nor broaden in the F1-T_2R complex.

stained with 2% uranyl acetate at 37 °C. Grids were examined using a Philips CM12 electron microscope. Images were recorded at ×13,000 and ×35,000 magnifications.

RESULTS

Tau Fragments Belonging to the Pro-rich and MTBR Domains Interact with Tubulin in T_2R—To identify Tau fragments that bind to tubulin, we have combined limited proteolysis of Tau and size exclusion chromatography (SEC) to select fragments that co-elute with the target. Because Tau, and potentially some of its fragments, favor the assembly of tubulin in MTs, this protein is not a useful target in these experiments as it would give rise to a heterogeneous population of oligomers that would not yield a well defined peak in SEC. Therefore, we have chosen as a target T_2R (36), which is not incorporated in MTs. Fragment F1 (Gly^{164}–Leu^{441}), devoid of the N-terminal projection domain that does not interact with the MT surface (44), was used to facilitate further the analysis of the results. We checked by SEC that F1 interacts with T_2R (supplemental Fig. S2). We previously showed that in the ^{1}H-^{15}N HSQC spectrum of F1 with stabilized MTs the only residues whose resonances maintain some intensity are at the C-terminal end of this fragment (32). To validate further T_2R as a target to investigate the Tau-tubulin interaction, it is important to ensure that F1 residues that interact with T_2R also interact with MTs. To do so, we recorded the NMR spectrum of F1 in complex with T_2R and compared it with that of F1 in its complex with stabilized MTs (Fig. 2). Residual intensity in the F1:MT spectrum is considerably lower than in the equivalent F1:T_2R spectrum reflecting that relaxation properties of the amide resonances are affected in a more drastic manner in the complex with MTs than with T_2R. This is likely due to the difference in molecular weight between the mesoscopic MTs and the 220-kDa T_2R and to the anisotropic tumbling of the rod-like MTs. Still, when resonances of residues at the C-terminal end of F1 were identified in the spectrum of the F1-T_2R complex, we found that they do not shift nor broaden (Fig. 2). This means that F1 residues that do not interact with MTs do not interact with T_2R either and, reciprocally, that residues that interact with T_2R should *a priori* interact with MTs.

The enzymes used for proteolysis, Arg-C and Glu-C, have a large number of cleavage sites evenly distributed along the F1 sequence (supplemental Fig. S1*A*). The enzyme/F1 ratio and digestion times were such that the molecular weights of resulting fragments are distributed over a wide range (for proteolysis details, see "Experimental Procedures" and supplemental Fig. S1). Fragments of F1 resulting from the digestion were submitted to SEC either on their own or mixed with T_2R. Elution was monitored at 280 nm, a wavelength at which in our conditions only tubulin absorbs, and at 230 nm to detect elution of F1 digestion products that have not been mixed with T_2R (in control experiments) or of unbound F1 peptides (data not shown) (Fig. 3*A*). SDS-PAGE analysis of eluted fractions demonstrates the co-elution of some digestion products with T_2R and, therefore, their binding (Fig. 3*B*). SEC fractions were also analyzed by MALDI-TOF MS (Glu-C cleavage see supplemental Table S1; Arg-C cleavage, data not shown). Proteolytic fragments of F1 were identified in fractions 3 and 4 of proteolyzed F1 eluted with T_2R. By contrast, the same fractions of proteolyzed F1 eluted on its own do not contain any fragment. Because these

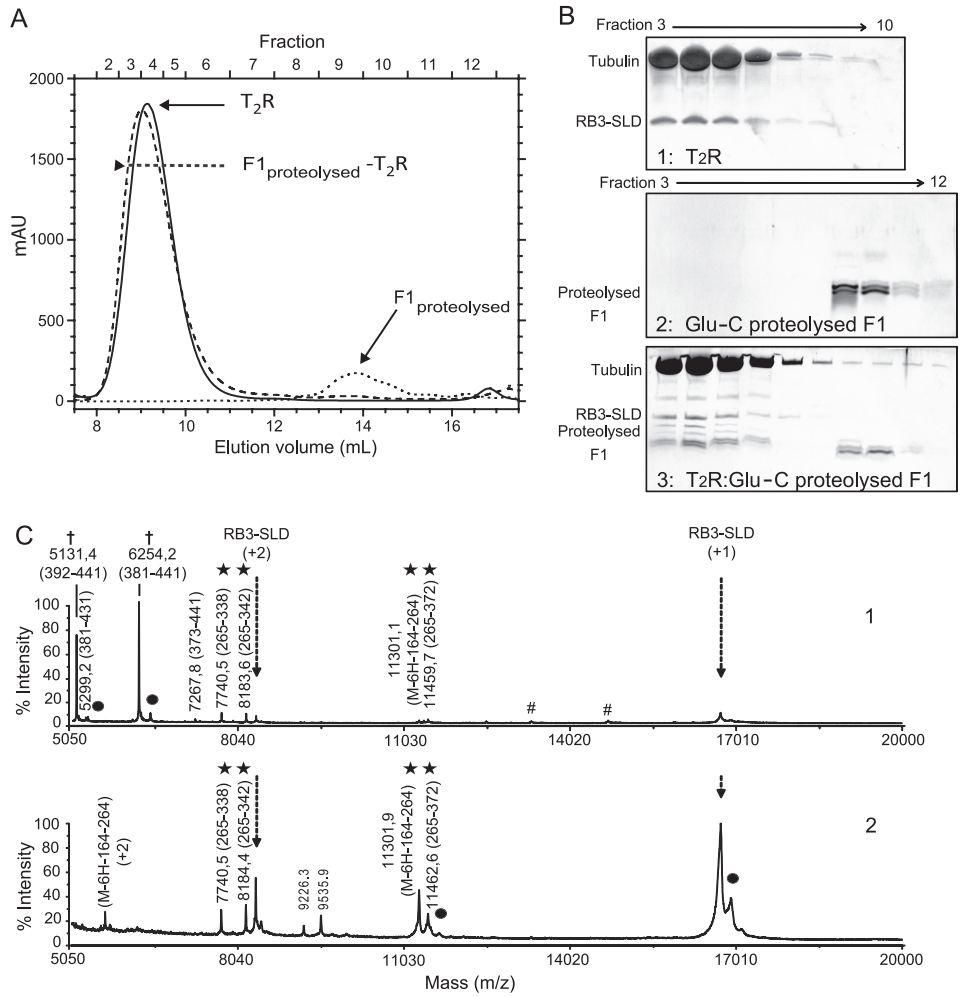

FIGURE 3. **Identification of F1 digestion products that interact with T_2R.** *A,* SEC profiles of T_2R (*solid line*), Glu-C proteolyzed F1 (*dotted line*), and of T_2R:Glu-C proteolyzed F1 (*dashed line*). Fractions defined at the *top* of this panel were submitted to SDS-PAGE analysis. *mAU*, milliabsorbance units. *B,* silver-stained Tricine-SDS-PAGE of eluted fractions of T_2R (*panel 1*), of F1 proteolyzed by Glu-C (*panel 2*), and of T_2R: proteolyzed F1 (*panel 3*). Low molecular weight peptides detected in fractions 3–6 of the SEC analysis of T_2R: proteolyzed F1 (*panel 3*) and absent in that of T_2R (*panel 1*) demonstrate co-elution of some of the F1 digestion products with T_2R. Note that some fragments of proteolyzed F1 that are hardly seen after SEC (compare *panel 2* with supplemental Fig. S1) become visible upon co-elution with T_2R, which also points to their interaction. *C,* identification by MALDI-TOF mass spectrometry of F1 peptides co-eluting with T_2R in SEC. Mass spectra of the T_2R-proteolyzed F1 complex before SEC (*panel 1*) and of fraction 4 of SEC elution of T_2R-proteolyzed F1 (*panel 2*) were recorded in linear mode. Four fragments (★) were detected in these two spectra but not in that corresponding to the analysis of the same fraction of the elution of proteolyzed F1 (data not shown). They interact specifically with T_2R. Note that spectra are scaled with respect to the highest peaks, which in *spectrum 1* corresponds to unbound peptides (†). As a consequence, the peaks corresponding to T_2R-interacting fragments appear very small in *spectrum 1* but not in the MS of SEC fraction 4 (*spectrum 2*). Differences between the theoretical and measured masses of F1 fragments are consistent with MALDI-TOF MS accuracy in the linear mode (between 0.01 and 0.05%). In the few cases where ambiguities arose, they were resolved by comparing results with F1 His-tagged at the N- and C-terminal ends. Matrix adducts (●) and Glu-C proteolyzed RB3-SLD fragments (#) are indicated. RB3-SLD (mono- and biprotonated) was used for internal calibration.

are the fractions where most T_2R is eluted, the fragments identified interact with T_2R. The spectrum of fraction 4 of T_2R: Glu-C proteolyzed F1 is shown as an example of the results obtained, together with that of the same sample before SEC (Fig. 3*C*, interacting fragments are noted with a *star*). Fig. 1*B* summarizes the location in the F1 sequence of fragments resulting from Arg-C or Glu-C proteolysis that were selected. Interacting fragments are localized in the proline-rich domain (*e.g.* 164–252 and 164–264, F2) and in the MTBR (*e.g.* 265–338 and 265–372, F3). Whereas some fragments in the SEC/MS screen, such as 164–372, also overlap these two regions, our results demonstrate that both the proline-rich and the MTBR domains, two separate regions of Tau, interact individually with T_2R. We used NMR analysis to define residues in these two regions that interact with T_2R. In addition, representative fragments among those we identified have been produced for further characterization; their limits are described in Fig. 1*B*.

NMR Analysis Identifies Residues of the Pro-rich and MTBR Domains That Mediate the Interaction with T_2R—To identify these residues, we used F2a (166–246) and K18 (244–372) (Fig. 1*B*) as they respectively compose the region of F2 in the Pro-rich domain (this work) and coincide with the MTBR (22). F2a was produced, and we confirmed by SEC/MS analysis that it interacts with T_2R (data not shown). $^{1}H,^{15}N$ HSQC spectra of F2a and K18 alone and with T_2R were recorded (Fig. 4). In the F2a spectra (Fig. 4*A*), the amide resonances of residues at the N terminus (*e.g.* Thr^{169}, Ile^{171}, Lys^{174}, and Thr^{181}) and at the C terminus (*e.g.* Arg^{209}, Thr^{220}, Ala^{227}, Val^{228}, Arg^{230}, Lys^{240}, and Ser^{241}) shift significantly in the presence of T_2R ($\Delta\omega$, as defined

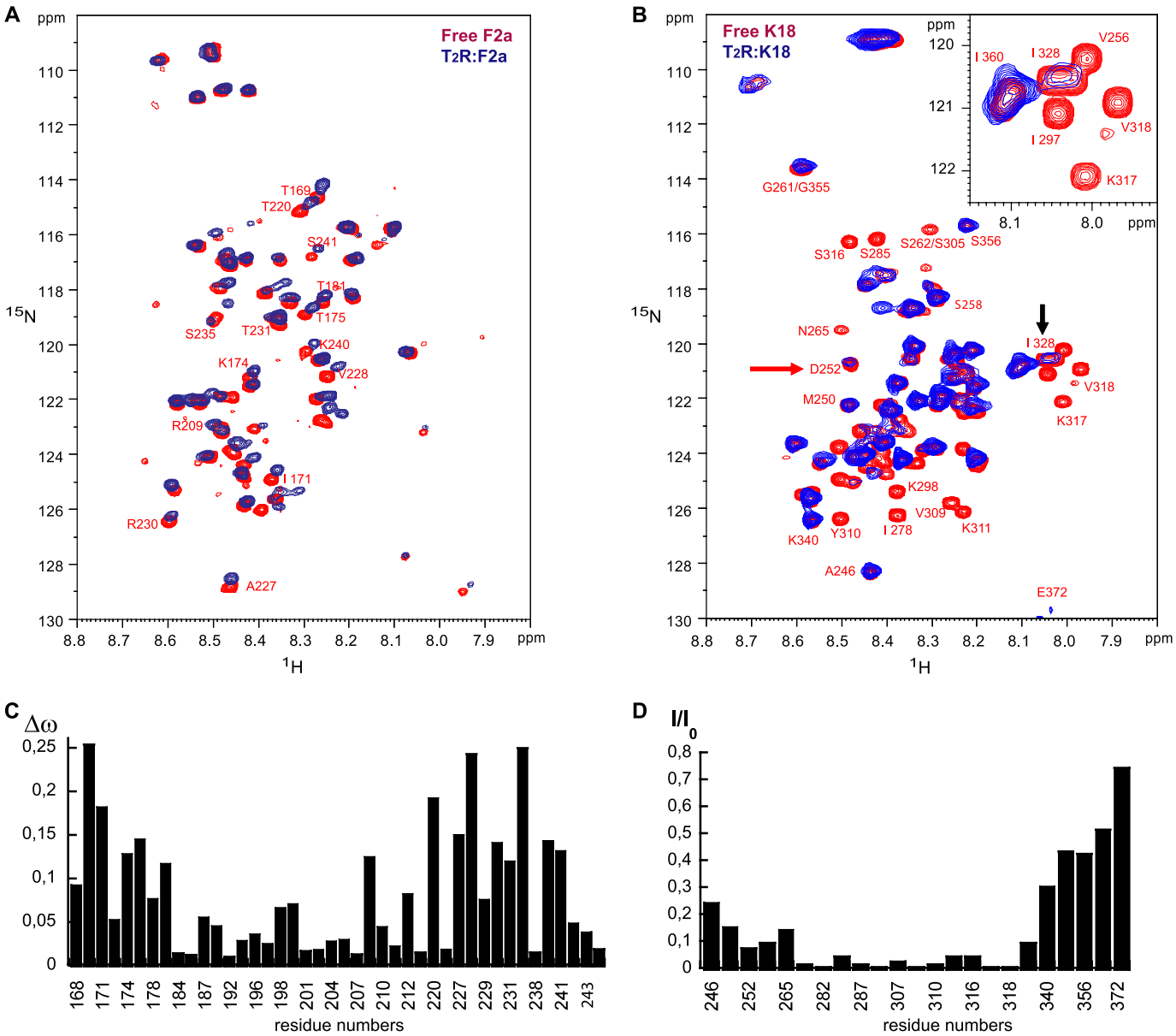

FIGURE 4. **NMR spectra of fragments F2a and K18.** ^{1}H-^{15}N HSQC spectra were recorded with the fragment alone (*red*) and in the presence of unlabeled T_2R (*blue*). *A,* F2a spectra; all residues for which $\Delta\omega$ ($\Delta\omega = (\Delta\omega_H^2 + 0.2\,\Delta\omega_N^2)^{1/2}$) is larger than 0.1 ppm are labeled. *B,* K18 spectra; resonances of residues between Asp^{252} and Ile^{328} (indicated by *arrows*) are broadened upon addition of T_2R. *C,* variations of the chemical shift of residues of F2a upon binding to T_2R. These show that the interacting region consists of two parts separated by a central peptide consisting of residues Ser^{184}–Ser^{208}. *D,* relative intensities of K18 resonances when in complex with T_2R compared with when it is free in solution.

under "Experimental Procedures," larger than 0.1 ppm), whereas almost no variation or variations of much smaller amplitude were observed for residues between these two regions (such as Gly^{186}, Gly^{192}, Gly^{196}, Tyr^{197}, and Thr^{205}) (Fig. 4*C*). Chemical shift mapping therefore allows the identification in F2a of two T_2R interacting regions separated by an unbound or loosely bound linker. The regions Thr^{169}–Thr^{181} and Arg^{209}–Ser^{241}, respectively, overlap motifs in PR1 and in PR2 for which a pronounced and strong signal broadening is observed upon MT or heparin binding (27, 31), and Arg^{209}–Ser^{241} contains basic residues (Lys^{224}, Lys^{225}, and Arg^{230}) that were found to contribute importantly to MT binding and assembly (24). Although the targets in these studies were T_2R (curved tubulin, this work) or MTs (straight tubulin), F2a and the proline-rich domain of Tau interact with these targets via similar residues. Moreover, the regions of the proline-rich domain that interact with tubulin do not depend on the presence of the MTBR in the fragment studied. In the K18 spectra, the amide resonances of all residues from Asp^{252} to Ile^{328} are severely broadened in the presence of T_2R (Fig. 4, *B* and *D*). In view of these results, we produced a new fragment, F4 (Ser^{208}–Ser^{324}) (Fig. 1), that includes the MTBR up to residue Ser^{324} (close to the C-terminal limit (Ile^{328}) of the region in K18 that interacts with T_2R) and the T_2R-interacting region of the proline-rich domain closest to the MTBR in Tau sequence.

Tau Fragments That Interact with T_2R Also Bind to Stabilized MTs—The interaction of Tau constructs with MTs was probed in a spin-down assay (Fig. 5*A*). Qualitatively, three

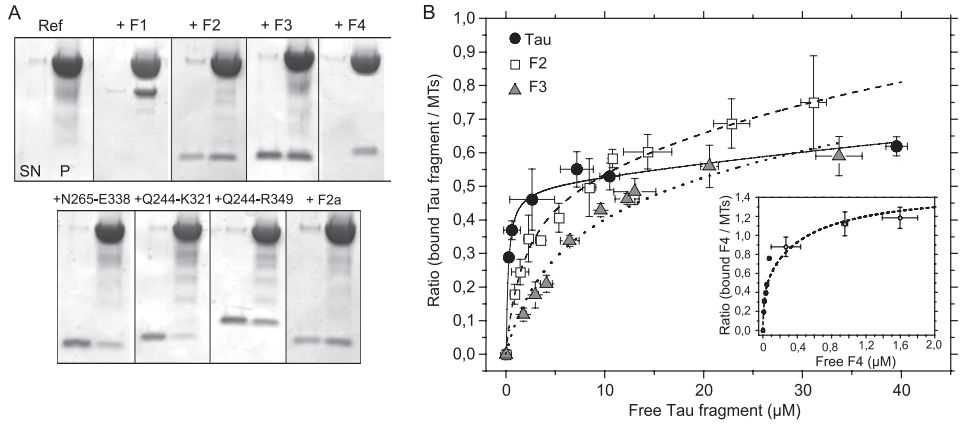

FIGURE 5. **Affinities of Tau fragments for stabilized MTs.** *A,* qualitative assay of the binding of Tau fragments to MTs by SDS-PAGE analysis of the tubulin and Tau fragment content in the pellet (*P*) and the supernatant (*SN*) after centrifugation of mixtures containing 10 μM tubulin in stabilized MTs and 5 μM Tau fragments. *B,* quantitative assay of the binding of Tau fragments to stabilized MTs. The same experiment as in *A* was repeated for variable concentrations of Tau fragments and 25 μM tubulin in MTs. Quantities of fragments in the supernatant (free fragment) and pellet (bound fragment) were determined as described under "Experimental Procedures." Because of the tight binding of F4 to MTs, its detection and the tubulin concentration (2 μM) were modified in this case; the results are shown in the *inset*. Variations of the ratio (bound fragments/MTs) as a function of free Tau fragments are presented and fitted with a two nonequivalent sites model (Equation 1, "Experimental Procedures").

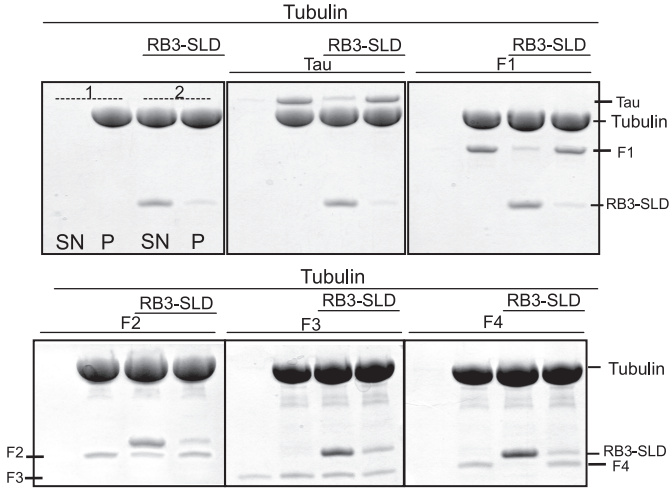

FIGURE 6. **Competitive binding of Tau fragments to stabilized MTs and T_2R.** The binding of Tau fragments was assayed in parallel to MTs (*panel 1*) and to MTs in the presence of an equal amount of tubulin in T_2R (*panel 2*). Samples were centrifuged and analyzed by SDS-PAGE as described (*SN,* supernatant; *P,* pellet). Tau, F1, and F4 bind preferentially to MTs in our conditions (and are almost exclusively in the pellet even in the presence of T_2R). Because some F2 is also found in the supernatant in the presence of T_2R (but not in its absence), the binding preference of F2 to MTs as compared with T_2R is less marked. Because of the moderate affinity of F3 for MTs, this assay of its competitive binding to MTs and T_2R does not lead to a clear conclusion.

groups of fragments may be distinguished. The first one includes the starting material (F1) and F4 that bind tightly to MTs and are quantitatively recovered in the pellet. Fragments in the second group (F2, F2a, (Gln^{244}–Arg^{349}), and F3) partition in the supernatant and the pellet, whereas the third group ((Gln^{244}–Lys^{321}) and (Asn^{265}–Glu^{338})) includes fragments with very low affinities for MTs; these are essentially recovered in the supernatant. K18 also belongs to the second group (data not shown). We characterized the fragments further in competition experiments (Fig. 6) in which MTs are assembled in the presence of RB3-SLD, in conditions such that, following centrifugation, the amounts of tubulin in the supernatant and the pellet are identical. Members of the first group have a higher affinity for stabilized MTs than for T_2R.

TABLE 1

Equilibrium constants (K_d) for the dissociation of Tau and its fragments from stabilized MTs

Data resulting from the quantification of spin-down analysis by SDS-PAGE, as presented in Fig. 5*B*, were fitted with a two-independent sites model as described under "Experimental Procedures." K_d^1 and K_d^2 are the equilibrium dissociation constants at these two sites. The stoichiometry of the tighter binding site, which was a parameter in the fit, was found to be one Tau fragment/two tubulin heterodimers.

Fragment	K_d^1	K_d^2
	μM	μM
Tau(1–441)	0.22 ± 0.04	252 ± 50
F2(164–264)	1.8 ± 0.2	81 ± 6
F2a(166–246)	3.1 ± 0.4	271 ± 43
F3(265–372)	5 ± 0.9	141 ± 25
F4(208–324)	<0.04[a]	0.5 ± 0.06[a]
K18(244–372)	10.7 ± 3	57 ± 11

[a] This was measured with 2 μM MTs.

This also applies to F2, in the second group. Results for fragments with a weaker affinity for MTs, such as F3, are more difficult to interpret as even in the absence of T_2R some material is found in the supernatant, unbound to MTs. Finally, we measured equilibrium constants for the dissociation from MTs of the tightest binding fragments we have identified in a spin-down assay by quantifying the amount of protein bound to MTs and in the supernatant (Fig. 5*B* and Table 1). For comparison with data from the literature, we also measured the K_d value of Tau and found it to be consistent with what has been measured using the same approach (22, 45). Data were best fitted with two nonequivalent binding sites, the higher affinity one consisting of two tubulin heterodimers. The stoichiometry of the low affinity site is less strictly defined by our data; we fixed it to one Tau fragment per tubulin. The resulting binding equilibrium equation (Equation 1) is equivalent to that used by Ackmann *et al.* (45) when the K_d value of the low affinity site is larger than the free fragment concentration. We did not study this site any further as the affinity of all the fragments we produced is more than 1 order of magnitude weaker than that for their tighter binding site (Table 1).

The K_d value of the high affinity site of fragments in the second group (Fig. 5*B*) are in the 1–10 μM range, and those of

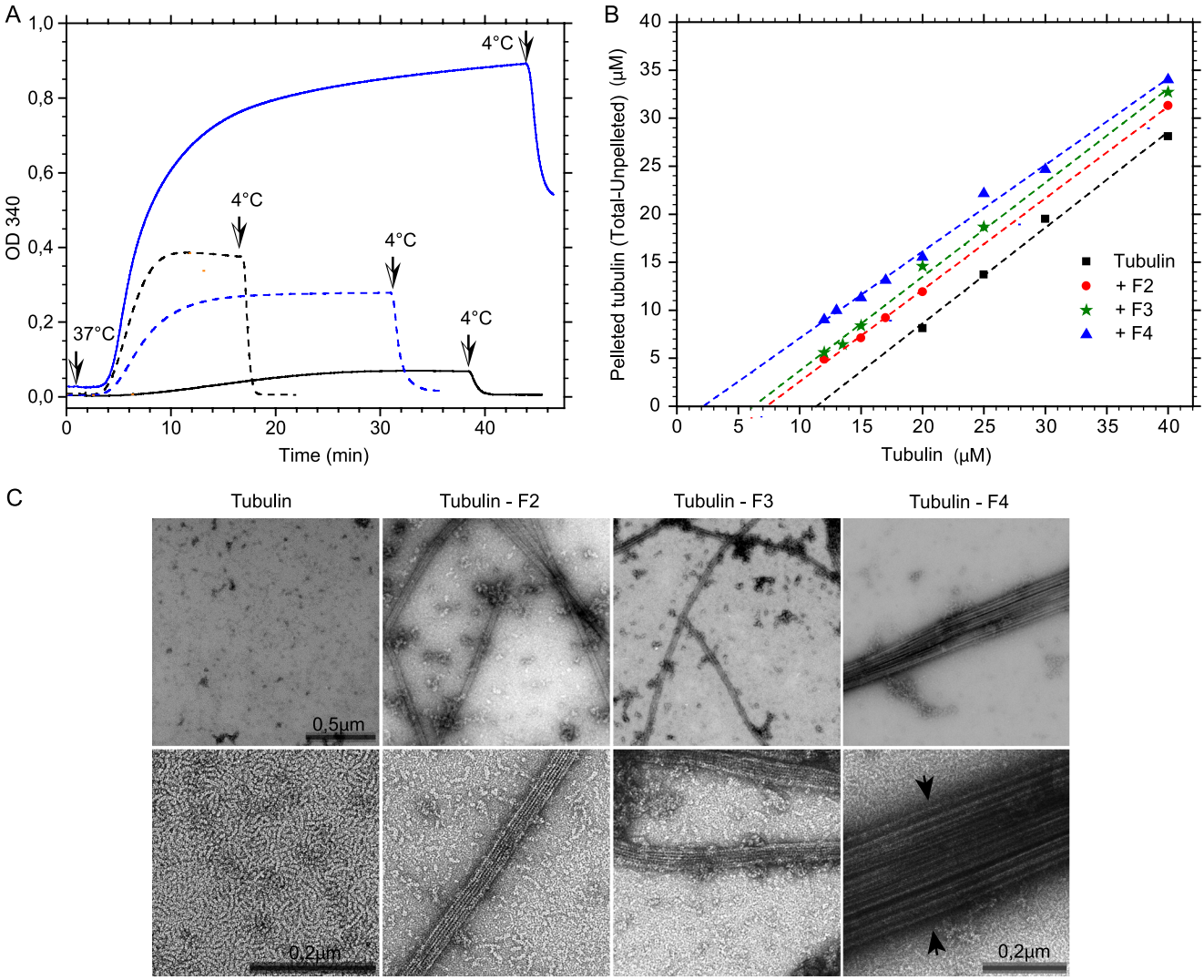

FIGURE 7. **Tau fragments promote microtubule assembly.** *A,* turbidity plots. MT assembly was carried out in buffer M2G1 from tubulin (*black*; 20 μM, *solid line*; 30 μM, *dashed line*) and from tubulin (12 μM) in the presence of F4 (1 μM, *blue dashed line* and 5 μM, *blue solid line*). *Arrows* indicate temperature steps (all heating steps were at the same time point). *B,* critical concentration plots in buffer M2G1 in the absence (■) or in the presence of Tau fragments (5 μM F2, *red circles*; F3, *green stars*; F4, *blue triangles*). *C,* electron micrographs of tubulin samples (13 μM), alone and with 5 μM F2, F3, and F4. Two magnifications were used, ×13,000 (*upper lane*) and ×35,000 (*lower lane*). *Arrows* point to MT bundles. No MT is observed in the absence of Tau fragments.

members of the third group were too high to be determined. Our results (Table 1) demonstrate that fragments identified in our screen for binding to T_2R, in which tubulin is curved (36), also interact with straight tubulin in MTs. The proline-rich domain taken individually (represented by F2 and F2a) binds to MTs with a dissociation constant in the micromolar range, which corresponds to an interaction slightly tighter than that of the MTBR domain (represented by F3 and K18). Moreover, the affinity for MTs of constructs included in the MTBR domain decreases significantly when they contain less than three repeats (Gln^{244}–Lys^{321} and Asn^{265}–Glu^{338}) (Fig. 5*A*), as observed previously (46). All the affinities of the fragments we identified in the screen are significantly weaker than that of Tau (or F1). This does not apply to F4, which was designed based on the results of the screen and on NMR data. To allow its affinity for MTs to be measured, we increased the sensitivity of its detection in binding studies by labeling it with a fluorescent probe. Despite that, the K_d value of the high affinity site on MTs for F4 can only be estimated to be lower than 0.04 μM (Table 1), as in the conditions of our assay this fragment totally segregates with MTs up to the saturation of that site (Fig. 5*B*). Therefore, a high affinity is restored by associating residues in the proline-rich region and in the MTBR domain.

Tight Tubulin Binding Fragments of Tau Promote MT Assembly—The effect on MT assembly of the fragments we characterized was also tested by determining the tubulin Cc when MTs are assembled in their presence (Fig. 7). Whereas the fragments with the lowest affinity for MTs (Gln^{244}–Lys^{321} and Asn^{265}–Glu^{338}) had very little effect if any at all (data not shown), all the others decreased Cc. In Fig. 7*B*, we present the effects of F4 and of F2 and F3, respectively in the proline-rich domain and MTBR region, which have the highest affinity for MTs among the fragments in these regions that we have characterized. To rule out the effects of MT bundling on the measurement of the mass of MTs, we did not use turbidity. Instead, we directly measured the quantity of tubulin in the supernatant following centrifugation after the steady state of MT assembly

had been reached (Fig. 7*A*) and deduced from the difference between total and soluble tubulin the quantity assembled. This is particularly important in the case of F4, as this fragment obviously induces MT bundling (Fig. 7*C*). In the graphical representation of the variation of assembled tubulin as a function of total tubulin concentration, Cc is given by the intersection of the regression line and the abscissa axis. We find that the three fragments decrease Cc, in agreement with the observation by electron microscopy of MTs in the presence of Tau fragments in conditions where no MT is seen with tubulin alone (Fig. 7*C*). F4, which has the highest affinity for MTs, has the largest effect (Fig. 7*B*).

DISCUSSION

The objective of this work was the identification of Tau fragments that bind to tubulin or MTs to facilitate structural studies and to dissect the mechanism by which Tau promotes MT assembly. We have found fragments in the proline-rich and MTBR regions of Tau (Fig. 1*B*) that each individually bind to T_2R, a soluble assembly of two tubulin heterodimers. Taken together, these fragments globally coincide with those previously proposed to mediate the Tau-MTs interaction (22, 24, 28, 29). The main difference is that the proline-rich region binds to T_2R and MTs, although this has not been reported by those who have included it in their studies (22, 23, 46). This discrepancy may appear because it was associated with the N-terminal extension when its binding was studied. It is possible that this extension, which is negatively charged, weakens the binding to the negative surface of MTs of the positive proline-rich region. The equilibrium constants for dissociation from MTs of the fragments included in the MTBR or proline-rich regions that we identified are in the 1–10 μM range. But when two peptides from these regions are combined in a single protein, as in F4, the resulting construct binds much tighter, which in particular allows it to stabilize MTs efficiently. Our results partially agree with the propositions made within the "jaws model." In this model, the Pro-rich, MTBR, and C-terminal extension domains all bind very weakly, if at all, to MTs, and the binding is considerably enhanced when two consecutive domains are associated in a single protein. Such combinations stabilize MTs and favor their assembly, but a combination without repeats is unproductive (22). We show that the Pro-rich and MTBR domains each bind weakly to MTs (Table 1), that each of them favors MTs assembly on its own (Fig. 7), and that the strongest binder (F4) generated by linking two peptides from these regions stimulates MT assembly more efficiently. We did not select any tubulin-binding fragment in the C-terminal extension of Tau, which may be due to the selection that was for soluble tubulin binding, as opposed to MT binding. We also note that the MTBR region included in F4 mostly corresponds to the MT binding core initially proposed by Feinstein and co-workers (28).

Interestingly, although the fragments we identified were selected because they bind to curved tubulin in T_2R, most of them also bind to straight tubulin in MTs (Fig. 5*A* and Table 1) and the tightest binding ones favor MT assembly, as Cc decreases when MTs are assembled in their presence (Fig. 7*B*). The mechanism by which this is achieved is best understood in the case of a protein (P) that binds in a 1:1 ratio to tubulin in solution as well as to tubulin incorporated in MTs, as described in Scheme 1, where Cc (resp. Cc^P) is the inverse of the tubulin-MT association constant in the absence (resp. presence) of protein (P), and K_1 and K_2 are the equilibrium constants for the association of this protein with tubulin in solution and in MTs. Because of the thermodynamic cycle above, and provided that P interacts equally with GDP- and GTP-tubulin, the following is verified as shown in Equation 2,

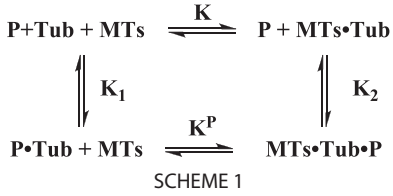

SCHEME 1

$$K_1/K_2 = Cc^P/Cc \qquad \text{(Eq. 2)}$$

Thus, if protein (P) binds with a higher affinity to tubulin in MTs than to tubulin in solution, Cc is decreased when MTs are assembled in its presence. In the case of Tau or its fragments, the situation is more complicated as they do not bind to tubulin in a 1:1 ratio. Nevertheless, one expects the conclusion above to hold true qualitatively. The binding to soluble tubulin of any protein that favors MT assembly is difficult to disentangle from MT assembly. Therefore, we compared the binding of Tau fragments to tubulin in MTs and in T_2R. F4 binds with a higher affinity to the former. This is also true, but to a lesser extent, for F2 and less clear for F3, whose affinity for MTs is weaker (Table 1). We also found that F2 and F3 decrease Cc less efficiently than F4 (Fig. 7*B*). It is therefore tempting to conclude, at least in the case of F2 and F4, that binding to T_2R reflects to some extent binding to soluble tubulin and that Cc is decreased when MTs are assembled in their presence because they bind tighter to tubulin in MTs than to soluble tubulin.

The stoichiometry of the tighter binding site of Tau and its fragments on tubulin in MTs has been determined when their affinities were measured; it consists of two tubulin heterodimers (Fig. 5*B* and Table 1), as does the binding site of stathmin family proteins. But the effect on MT assembly of the proteins studied here differs radically from that of stathmin family proteins, which constitute with tubulin a complex that is not incorporated in MTs and does not assemble any further (35, 47). F4, the tightest binder and one of the shortest fragments we produced, is best suited to structural studies. Structural characterization of the interaction of F4 with tubulin is required to define better the transient complex that is formed and to elucidate the basis for the opposite effects of this Tau fragment and stathmin family proteins. Furthermore, determination of the structure of functional complexes mimicking the interaction of Tau with tubulin will be essential to document the molecular mechanisms by which Tau promotes MT assembly.

Acknowledgments—We are indebted to Ingrid Mignot and Ludovic Pecqueur for their help in the experimental work, to Lionel Cladière for providing us with an F4 construct, and to Juan Lopez for help with Fig. 4. We thank Marie-France Carlier for insightful discussions, Vincent Guérineau (Laboratoire de Spectrométrie de Masse, Institut de Chimie des Substances Naturelles, Gif-sur-Yvette) for advice during MS data recording, and Jean Lepault (Virologie Moléculaire et Structurale, CNRS, Gif-sur-Yvette) for electron microscopy. The NMR facilities are funded by the European Community, the CNRS, the Région Nord-Pas de Calais (France), the University of Lille 1, and the Institut Pasteur de Lille.

REFERENCES

1. Desai, A., and Mitchison, T. J. (1997) *Annu. Rev. Cell Dev. Biol.* **13,** 83–117
2. van der Vaart, B., Akhmanova, A., and Straube, A. (2009) *Biochem. Soc. Trans.* **37,** 1007–1013
3. Binder, L. I., Frankfurter, A., and Rebhun, L. I. (1985) *J. Cell Biol.* **101,** 1371–1378
4. Black, M. M., Slaughter, T., Moshiach, S., Obrocka, M., and Fischer, I. (1996) *J. Neurosci.* **16,** 3601–3619
5. Dehmelt, L., and Halpain, S. (2005) *Genome Biol.* **6,** 204
6. Avila, J. (2010) *Front. Neurosci.* **4,** 49
7. Avila, J., Lucas, J. J., Perez, M., and Hernandez, F. (2004) *Physiol. Rev.* **84,** 361–384
8. Brandt, R., Hundelt, M., and Shahani, N. (2005) *Biochim. Biophys. Acta* **1739,** 331–354
9. Hernández, F., and Avila, J. (2007) *Cell. Mol. Life Sci.* **64,** 2219–2233
10. Iqbal, K., Liu, F., Gong, C. X., Alonso Adel, C., and Grundke-Iqbal, I. (2009) *Acta Neuropathol.* **118,** 53–69
11. Cleveland, D. W., Hwo, S. Y., and Kirschner, M. W. (1977) *J. Mol. Biol.* **116,** 227–247
12. Schweers, O., Schönbrunn-Hanebeck, E., Marx, A., and Mandelkow, E. (1994) *J. Biol. Chem.* **269,** 24290–24297
13. Goedert, M., Spillantini, M. G., Jakes, R., Rutherford, D., and Crowther, R. A. (1989) *Neuron* **3,** 519–526
14. Himmler, A. (1989) *Mol. Cell. Biol.* **9,** 1389–1396
15. Himmler, A., Drechsel, D., Kirschner, M. W., and Martin, D. W., Jr. (1989) *Mol. Cell. Biol.* **9,** 1381–1388
16. Brandt, R., Léger, J., and Lee, G. (1995) *J. Cell Biol.* **131,** 1327–1340
17. Weissmann, C., Reyher, H. J., Gauthier, A., Steinhoff, H. J., Junge, W., and Brandt, R. (2009) *Traffic* **10,** 1655–1668
18. Chen, J., Kanai, Y., Cowan, N. J., and Hirokawa, N. (1992) *Nature* **360,** 674–677
19. Kanai, Y., Chen, J., and Hirokawa, N. (1992) *EMBO J.* **11,** 3953–3961
20. Mukhopadhyay, R., and Hoh, J. H. (2001) *FEBS Lett.* **505,** 374–378
21. Rosenberg, K. J., Ross, J. L., Feinstein, H. E., Feinstein, S. C., and Israelachvili, J. (2008) *Proc. Natl. Acad. Sci. U.S.A.* **105,** 7445–7450
22. Gustke, N., Trinczek, B., Biernat, J., Mandelkow, E. M., and Mandelkow, E. (1994) *Biochemistry* **33,** 9511–9522
23. Brandt, R., and Lee, G. (1993) *J. Biol. Chem.* **268,** 3414–3419
24. Goode, B. L., Denis, P. E., Panda, D., Radeke, M. J., Miller, H. P., Wilson, L., and Feinstein, S. C. (1997) *Mol. Biol. Cell* **8,** 353–365
25. Preuss, U., Biernat, J., Mandelkow, E. M., and Mandelkow, E. (1997) *J. Cell Sci.* **110,** 789–800
26. Trinczek, B., Biernat, J., Baumann, K., Mandelkow, E. M., and Mandelkow, E. (1995) *Mol. Biol. Cell* **6,** 1887–1902
27. Mukrasch, M. D., von Bergen, M., Biernat, J., Fischer, D., Griesinger, C., Mandelkow, E., and Zweckstetter, M. (2007) *J. Biol. Chem.* **282,** 12230–12239
28. Goode, B. L., Chau, M., Denis, P. E., and Feinstein, S. C. (2000) *J. Biol. Chem.* **275,** 38182–38189
29. Goode, B. L., and Feinstein, S. C. (1994) *J. Cell Biol.* **124,** 769–782
30. Chau, M. F., Radeke, M. J., de Inés, C., Barasoain, I., Kohlstaedt, L. A., and Feinstein, S. C. (1998) *Biochemistry* **37,** 17692–17703
31. Mukrasch, M. D., Bibow, S., Korukottu, J., Jeganathan, S., Biernat, J., Griesinger, C., Mandelkow, E., and Zweckstetter, M. (2009) *PLoS Biol.* **7,** e34
32. Sillen, A., Barbier, P., Landrieu, I., Lefebvre, S., Wieruszeski, J. M., Leroy, A., Peyrot, V., and Lippens, G. (2007) *Biochemistry* **46,** 3055–3064
33. Cao, B., and Mao, C. (2009) *Biomacromolecules* **10,** 555–564
34. Redeker, V., Lachkar, S., Siavoshian, S., Charbaut, E., Rossier, J., Sobel, A., and Curmi, P. A. (2000) *J. Biol. Chem.* **275,** 6841–6849
35. Gigant, B., Curmi, P. A., Martin-Barbey, C., Charbaut, E., Lachkar, S., Lebeau, L., Siavoshian, S., Sobel, A., and Knossow, M. (2000) *Cell* **102,** 809–816
36. Ravelli, R. B., Gigant, B., Curmi, P. A., Jourdain, I., Lachkar, S., Sobel, A., and Knossow, M. (2004) *Nature* **428,** 198–202
37. Amniai, L., Barbier, P., Sillen, A., Wieruszeski, J. M., Peyrot, V., Lippens, G., and Landrieu, I. (2009) *FASEB J.* **23,** 1146–1152
38. Castoldi, M., and Popov, A. V. (2003) *Protein Expr. Purif.* **32,** 83–88
39. Correia, J. J., Baty, L. T., and Williams, R. C., Jr. (1987) *J. Biol. Chem.* **262,** 17278–17284
40. Detrich, H. W., 3rd, and Williams, R. C. (1978) *Biochemistry* **17,** 3900–3907
41. Charbaut, E., Curmi, P. A., Ozon, S., Lachkar, S., Redeker, V., and Sobel, A. (2001) *J. Biol. Chem.* **276,** 16146–16154
42. Charbaut, E., Redeker, V., Rossier, J., and Sobel, A. (2002) *FEBS Lett.* **529,** 341–345
43. Verdegem, D., Dijkstra, K., Hanoulle, X., and Lippens, G. (2008) *J. Biomol. NMR* **42,** 11–21
44. Steiner, B., Mandelkow, E. M., Biernat, J., Gustke, N., Meyer, H. E., Schmidt, B., Mieskes, G., Söling, H. D., Drechsel, D., Kirschner, M. W., *et al.* (1990) *EMBO J.* **9,** 3539–3544
45. Ackmann, M., Wiech, H., and Mandelkow, E. (2000) *J. Biol. Chem.* **275,** 30335–30343
46. Butner, K. A., and Kirschner, M. W. (1991) *J. Cell Biol.* **115,** 717–730
47. Jourdain, L., Curmi, P., Sobel, A., Pantaloni, D., and Carlier, M. F. (1997) *Biochemistry* **36,** 10817–10821